Atmospheric
Chemistry
and Physics
Discussions

Open Access

Size-dependent particle activation properties in fog during the ParisFog 2012/13 field campaign

E. Hammer[1], M. Gysel[1], G. C. Roberts[2,3], T. Elias[4], J. Hofer[1], C. R. Hoyle[1,5], N. Bukowiecki[1], J.-C. Dupont[6], F. Burnet[2], U. Baltensperger[1], and E. Weingartner[1,*]

[1]Laboratory of Atmospheric Chemistry, Paul Scherrer Institute, 5232 Villigen PSI, Switzerland
[2]CNRM/GAME – Meteo-France/CNRS, 42 av. Gaspard Coriolis, 31057 Toulouse, France
[3]Scripps Institution of Oceanography, 9500 Gilman Dr., La Jolla CA 92093, USA
[4]Hygeos, 165 Avenue de Bretagne, 59000 Lille, France
[5]Swiss Federal Institute for Forest Snow and Landscape Research (WSL)-Institute for Snow and Avalanche Research (SLF), 7270 Davos, Switzerland
[6]Institut Pierre-Simon Laplace, Université Versailles Saint Quentin, 78280 Guyancourt, France
[*]now at: Institute for Aerosol and Sensor Technology, University of Applied Sciences, 5210 Windisch, Switzerland

ACPD

14, 9475–9516, 2014

Particle activation properties in fog

E. Hammer et al.

Title Page

Abstract	Introduction
Conclusions	References
Tables	Figures

|◄ | ►|

◄ | ►

Back | Close

Full Screen / Esc

Printer-friendly Version

Interactive Discussion

ACPD

14, 9475–9516, 2014

Particle activation properties in fog

E. Hammer et al.

Back | Close

Full Screen / Esc

Printer-friendly Version

Interactive Discussion

Abstract

Fog causes a variety of hazards in road traffic, maritime navigation, as well as in air traffic and railway traffic. There is a great demand, e.g. from airports, for more reliable fog forecasts to prevent fog related accidents. Improved fog forecasts require a better understanding of the numerous complex mechanisms during the fog life cycle. During winter 2012/13 a field campaign called ParisFog aiming at fog research took place at SIRTA (Instrumented Site for Atmospheric Remote Sensing Research). SIRTA is located about 20 km southwest of the Paris city centre, France in a semi-urban environment. In situ activation properties of the prevailing fog were investigated by measuring: (1) total and interstitial (non-activated) dry particle number size distributions behind two different inlet systems; (2) interstitial hydrated aerosol and fog droplet size distributions at ambient conditions; (3) cloud condensation nuclei (CCN) number concentration at different supersaturations (SS) with a CCN counter. The aerosol particles were characterized regarding their hygroscopic properties, fog droplet activation behavior and contribution to light scattering for 17 developed fog events. Low particle hygroscopicity with an overall median of hygroscopicity parameter, κ, of 0.14 was found, likely caused by substantial influence from local traffic and wood burning emissions. Measurements of the aerosol size distribution at ambient RH revealed that the critical wet diameter, above which the hydrated aerosols activate to fog droplets, is rather large with a median value of 2.4 μm and is highly variable (ranging from 1 to 5 μm) between the different fog events. Thus, the number of activated fog droplets was very small and the non-activated hydrated particles were found to contribute siginifically to the observed light scattering and thus to the reduction in visibility. Combining all experimental data, the effective peak supersaturation, SS_{peak}, a measure of the peak supersaturation during the fog formation, was determined. The median SS_{peak} value was estimated to be in the range from 0.031 to 0.046 % (upper and lower limit estimations), which is in good agreement with previous experimental and modeling studies of fog.

1 Introduction

Hygroscopicity is defined as the ability of aerosol particles to take up water. This water uptake plays an important role in the Earth's radiative budget as it changes the particle's light scattering and absorption properties. The interaction of aerosol with solar radiation can either be direct, or through the aerosol's modification of cloud properties. Aerosols influencing fog are also a major factor in visibility reduction at surface levels, which can cause fatalities in traffic (Rosenfeld, 1996). When the relative humidity increases, particles can grow substantially and if the atmosphere gets supersaturated with water vapor, particles can activate to form fog droplets (e.g., Bergot, 2007), depending on their size and hygroscopic properties. The term mist is used if visibility drops below 5 km (Vautard et al., 2009) and the term fog is used below a visibility threshold of 1 km (Tardif and Rasmussen, 2007; Maier et al., 2013). Studies in Europe showed that during developed fog the visibility can decrease down to 50 m and lower (e.g., David et al., 2013; Elias et al., 2009).

In the recent years, several field campaigns were carried out in Europe and North America focusing on physical and chemical processes in continental fog (Gultepe et al., 2007). Some studies investigated a certain fog type such as radiation fog in the Fog-82 campaign in Albany, New York (Meyer et al., 1986), or radiation fog in the Lille-88 and Lille-91 field experiments in northern France (Guedalia and Bergot, 1994). The role of turbulence in fog formation was studied at the Cabauw station in the Netherlands (Duynkerke, 1991). In the years 1989 and 1998, field campaigns were performed in the Po Valley, Italy (Heintzenberg, 1992) investigating the fog microphysical processes (Noone et al., 1992b; Svenningsson et al., 1992) and the evolution of chemical species in the observed air masses (Facchini et al., 1992; Fuzzi et al., 1992). In the winter 2006/2007, the series of ParisFog field campaigns started to monitor important processes for fog formation and dynamics simultaneously (Haeffelin et al., 2010). This study presents results from the latest ParisFog campaign which was conducted in winter 2012/2013.

Despite the advances in modeling (e.g., Bott et al., 1990; Stolaki et al., 2012), the representation of the physical processes leading to fog formation has not yet progressed to the point where numerical models can accurately forecast/nowcast the fog events (Gultepe et al., 2007). The goals of this study are to examine the interaction between particles and fog, and the partitioning of water within this system to improve the understanding of fog formation.

Cloud condensation nuclei (CCN) activity can be defined by the particles' critical supersaturation (SS_{crit}), i.e., the lowest supersaturation at which the particles can activate to a fog or cloud droplet. The critical supersaturation depends on the size and chemical composition of the particle (McFiggans et al., 2006). Cooling of an air parcel to temperatures below its dew point will result in the formation of a cloud or fog, and those particles with a critical supersaturation below the peak supersaturation in the cloud are activated to form cloud droplets. The effective peak supersaturation (SS_{peak}) of a cloud is defined as the highest supersaturation that a particle experiences for a sufficiently long time such that all particles with SS_{crit} smaller than SS_{peak} are able to grow to a stable cloud/fog droplet (Hammer et al., 2014). The term effective is used here because very short supersaturation spikes that do not lead to additional droplet activation of particles are irrelevant in this context. SS_{peak} is a key parameter for aerosol-to-cloud droplet activation and is thus an important quantity for fog and cloud parameterizations in models (e.g. Kim and Yum, 2012; Stolaki et al., 2012; Zhao et al., 2012). Those particles having a larger critical supersaturation than the peak supersaturation of the air parcel will remain non-activated in the hydrated aerosol mode. The largest size that particles can grow to while still being in stable equilibrium, is at their SS_{crit} and is defined by the particle's hygroscopic properties (Petters and Kreidenweis, 2007). These unactivated particles, however, grow to their stable equilibrium size by taking up water, remaining smaller than activated droplets, but large enough to contribute significantly to extinction (sum of scattering and absorption) of visible radiation in fog (Elias et al., 2009). The relative contribution of stable non-activated particles and activated particles to the light scattering is presented in this study.

Title Page

Abstract | Introduction

Conclusions | References

Tables | Figures

◄ | ►

◄ | ►

Back | Close

Full Screen / Esc

Printer-friendly Version

Interactive Discussion

CC BY

A detailed examination of the aerosol properties during fog occurrence was performed to determine which fraction of the total particles is activated to fog droplets (Sect. 4.1). The activation properties of the particles within fog are further investigated by comparing dry with ambient (humid) size distribution measurements. The effective peak supersaturation is quantified and discussed for the fog events observed at the SIRTA site (Sect. 4.2). The contribution of hydrated but non-activated particles to the visibility reduction during fog is also investigated and the relative contribution of stable non-activated particles and activated particles to the light scattering is presented (Sect. 4.3).

2 Experimental

2.1 ParisFog 2012/13 campaign

ParisFog is a series of field campaigns focusing on fog research (Haeffelin et al., 2010). They have taken place at the Instrumented Site for Atmospheric Remote Sensing Research (SIRTA) several times since 2006. SIRTA is located in the immediate vicinity of the Ecole Polytechnique Palaiseau, on the Saclay plateau about 20 km southwest of Paris city centre. The site is located in a semi-urban environment composed of roughly equal portions of agricultural fields, wooded areas, housing and industrial developments (Haeffelin et al., 2005). SIRTA hosts active and passive remote sensing instruments to continuously quantify cloud and particle properties, as well as key atmospheric parameters (Haeffelin et al., 2005). During the ParisFog 2012/13 campaign in the winter season (October to March), additional measurement instruments were provided and operated by several research institutes, as described below. During this time, the goal was to closely observe surface conditions, large- and small-scale dynamics, radiation, turbulence, precipitation, droplet- and particle-microphysics and -chemistry. The data presented in this study covers the time period from 2 October 2012 to 7 January 2013.

2.2 Instrumentation

The instrumentation used in this study is listed in Table 1. For the sampling of the particles and hydrometeors, a total and an interstitial inlet were installed on the roof of a measurement container at 4 m a.g.l. The total inlet collected all particles (including droplets). The water associated with the hydrometeors and aerosol particles was evaporated by heating the top part of this inlet to approximately 20 °C, and subsequently all dried aerosol particles (non-activated aerosols and the residuals of the fog droplets) reached the instruments in the laboratory. The interstitial inlet sampled particles with an aerodynamic diameter smaller than 1 µm at ambient RH (from 17 October 2012 07:00 to 14 November 2012 16:00 UTC). This size cut was changed to 2 µm from 2 October 2012 17:00 to 17 October 2012 07:00 UTC and from 14 November 16:00 to 7 January 2012 15:00 UTC. This inlet consists of an aerodynamic size discriminator (PM$_{2.5}$, Very Sharp Cut Cyclone, BGI, USA and PM$_1$, Sharp Cut Cyclone 2.229, BGI Inc.) running at flow rates of ∼ 20 lpm (PM$_2$) or ∼ 16 lpm (PM$_1$). The term interstitial is based on the assumption that all particles larger than the applied cut-off consist of activated cloud droplets. However, this was not always the case, particularly when the smaller cut-off diameter of 1 µm was applied, as discussed in Sect. 4.2.

Inside the container the dried number size distributions of total and interstitial particles were measured with a scanning mobility particle sizer (SMPS) consisting of a differential mobility analyzer (DMA; TSI 3071) and a condensation particle counter (TSI CPC 3022). The DMA was operated at a sample air flow rate of 0.3 lpm and a closed loop excess and sheath air setup with a flow rate of 3 lpm. The measured mobility diameters ranged from 13 nm to 520 nm. The scan time of one size distribution was 6 min and after each scan the instrument was automatically switched between the total and interstitial inlets. During fog-free periods the two SMPS systems should measure identical dry aerosol number size distributions. However, the measured size distributions showed average differences of up to 15 % in concentration (in the size range of 13 to 520 nm) due to the changes in air masses between the two scans. To eliminate the

small differences between the two size distribution measurements in the calculation of the activated fraction (Sect. 3.6), the total size distribution was scaled to equal the average of the two interstitial size distributions measured immediately before and after.

To measure the cloud condensation nuclei (CCN) number concentration, a miniature continuous flow streamwise thermal gradient CCN chamber (m-CCNC; Sullivan et al., 2009) was installed downstream of the total inlet. This instrument was constructed at Scripps Institution of Oceanography based on the design of Roberts and Nenes (2005). The particles sampled behind the total inlet are introduced to the center of a column surrounded by a sheath of filtered humidified air. A linear temperature gradient along the column produces a well-defined and controlled supersaturation (SS) with respect to water. The SS is defined by the temperature gradient and the flow rate. Particles that take up water and grow to a diameter size of > 1 μm are detected by an optical particle counter at the end of the column and are counted as CCN. The temperature differences and flow rate were scanned from 4 to 14 K and from 0.1 to 0.28 lpm, respectively, such that a SS range of 0.05 to 0.6 % was achieved (for the uncertainties, see Table 1). The m–CCNC was calibrated before and after the campaign using monodisperse ammonium sulfate particles (nebulized from a solution, dried by a diffusion drier and size segregated by a DMA).

For the data analysis it is important to know when fog was present and especially how dense it was. For this task a Degreanne forward scatter sensor DF20+ was operated at a height of 3 m above the ground. The instrument provided a measurement of the horizontal visibility with a white light source (wavelength from 350 to 900 nm) and a receiver placed off axis from the source. In addition, a Particle Volume Monitor (PVM-100; Gerber, 1991) additionally measured the liquid water content (LWC) by forward light scattering.

An optical particle counter, WELAS 2000 (Palas Inc.), was used to measure the number size distribution of hydrated aerosol particles and fog droplets up to a diameter of ~ 10 μm at ambient conditions by means of light scattering (size range between 360 nm and 42 μm water droplet equivalent diameter). Droplets larger than ~ 10 μm

Particle activation properties in fog

E. Hammer et al.

Title Page

Abstract | Introduction

Conclusions | References

Tables | Figures

|◄ | ►|

◄ | ►

Back | Close

Full Screen / Esc

Printer-friendly Version

Interactive Discussion

could not be measured due to the inlet used with the WELAS 2000 (Burnet et al., 2012; Elias et al., 2014). The instrument was calibrated in the laboratory with monodisperse latex spheres (PSL; index of refraction = 1.59). During fog events, when the RH is $\sim 100\,\%$, the particles can be expected to be hydrated and mainly composed of water. Therefore, an index of refraction for water ($m = 1.333$) was used to infer correct particle/droplet sizes from the WELAS raw data. According to Heim et al. (2008), the detection efficiency is ~ 1 for $D(\text{PSL}) \gtrsim 1\,\mu\text{m}$, which translates to a water droplet diameter of $D(\text{droplet}) \sim 1.4\,\mu\text{m}$. Thus, only WELAS data having a $D(\text{droplet}) \gtrsim 1.4\,\mu\text{m}$ will be considered in this study.

3 Methods

3.1 Classification of fog types

According to Tardif and Rasmussen (2007) developed fog is defined by a visibility is lower than 1.6 km (1 land mile; however, in Europe it is common to use a threshold of 1 km; Haeffelin et al., 2010) for at least 30 min during a 50 min period. An automatic classification of fog events according to the scheme of Tardif and Rasmussen (2007) was carried out for the whole measurement period (2 October 2012 to 7 January 2013). The classification uses visibility, temperature, wind speed, precipitation, cloud cover and ceiling height as parameters to assign a type of fog to each event. The fog events were assigned to three different categories: (1) radiation fog (RAD) is mainly triggered by the balance of infrared radiative cooling and turbulent mixing which cools the bottom air layer until it reaches saturation. Further radiative cooling at the top of the fog layer deepens it at the surface layer (Haeffelin et al., 2010). (2) Stratus lowering fog (STL) is initiated by a stratus cloud layer. Due to the radiative cooling at the cloud top, larger cloud droplets settle downwards to and beyond cloud base, thus leading to a lowering of the cloud base (Dupont et al., 2012). (3) precipitation fog (PREC), or in some literature also called frontal fog, is formed by rain that falls from warmer air masses down to

colder air masses (subcloud layer) and evaporates. The corresponding evaporative cooling and additional water vapor leads to saturation and thus fog is able to form (Hupfer et al., 2005). However, precipitation fog occurred only once during the period covered in this study.

3.2 κ-Köhler theory

The equilibrium saturation vapor pressure (RH_{eq}) over a solution droplet is described by the Köhler theory (Köhler, 1936) considering the Raoult (solute) and Kelvin effects. Petters and Kreidenweis (2007) introduced a simple parameterization for the solute (Raoult) term in the Köhler equation. With this, the semi-empirical "κ-Köhler equation" is obtained (here expressed for the equilibrium supersaturation SS_{eq} as a function of the diameter of the solution droplet D):

$$SS_{eq}(D) := RH_{eq}(D) - 1 = \frac{D^3 - (D^{dry})^3}{D^3 - (D^{dry})^3(1-\kappa)} \exp\left(\frac{4\sigma_{s/a}M_w}{RT\rho_w D}\right) - 1 \qquad (1)$$

where D^{dry} is the dry particle diameter, $\sigma_{s/a}$ is the surface tension of solution/air interface (in our calculations the surface tension of pure water was taken), R is the universal gas constant, M_w is the molar mass of water, T is the absolute temperature, ρ_w is the density of water and κ is the hygroscopicity parameter, which depends on the particle chemical composition. Equation (1) provides the relationship between SS_{eq} (RH_{eq}), D^{dry}, D, and κ under equilibrium conditions, and forms the basis for various theoretical calculations done in the data analysis. For example, the critical superation (SS_{crit}) of a particle with a certain dry size (D^{dry}) and composition/hygroscopicity (κ) is obtained by numerically searching for the maximum of Eq. (1) as a function of the droplet diameter (D).

Particle activation properties in fog

E. Hammer et al.

3.3 Reproducing the ambient total size distribution from dry SMPS measurements

Figure 1 shows, as an example, the averaged total dry number size distribution (in brown) for a stratus lowering fog event on 12 November 2012. Since the total inlet samples the interstitial as well as the activated particles and dries them, all particles including droplet residuals are measured with the SMPS. With the assumption that the ambient relative humidity (RH) in the fog is approximately 100 %, the total dry size distribution measured by the SMPS (brown line in Fig. 1) was recalculated to the corresponding ambient wet size distribution assuming hydrated (non-activated) particles (blue line in Fig. 1) using κ-Köhler theory (Petters and Kreidenweis, 2007, see also Sect. 3.2) and a fixed κ value of 0.14 (overal median kappa value discussed in Sect. 4.1). The recalculated SMPS size distribution distribution is comparable to the WELAS measurement of the size distribution at ambient RH (see green line in Fig. 1) in the common size range of 1.4 to 2.6 µm, which is a strong indication that the majority of these particles are not activated but hydrated particles in stable equilibrium. The total ambient size distribution for the complete diameter range 17 nm to $\sim$ 10 µm was obtained by merging the recalculated SMPS measurement with the WELAS measurement, whereby the recalculated SMPS measurements were taken up to a diameter of 1 µm and the WELAS measurement covered the size range from 1 µm to 10 µm.

3.4 Retrieving the light scattering coefficients

To investigate the influence of hydrated particles and fog droplets on the light scattering during the fog events, the light scattering coefficient size distribution $\left(\frac{\mathrm{d}b_{\mathrm{s}}}{\mathrm{dlog}D^{\mathrm{wet}}}\right)$ was calculated from the ambient wet number size distribution $\frac{\mathrm{d}N^{\mathrm{wet}}}{\mathrm{dlog}D^{\mathrm{wet}}}$:

$$\frac{\mathrm{d}b_s(D^{\mathrm{wet}})}{\mathrm{dlog}D^{\mathrm{wet}}} = \sigma(D^{\mathrm{wet}}) \cdot \frac{\mathrm{d}N^{\mathrm{wet}}(D^{\mathrm{wet}})}{\mathrm{dlog}D^{\mathrm{wet}}} \tag{2}$$

where $\sigma(D^{\text{wet}})$ is the scattering cross section for the solar spectrum (American Society for Testing and Materials (ASTM); www.astm.org/) of a spherical water droplet with diameter D^{wet} and a refractive index of $m = 1.333 - 0i$. The total light scattering coefficient, b_s, is then obtained by integrating $\frac{db_s}{d\log D^{\text{wet}}}$ over the whole diameter range.

3.5 Retrieving the threshold wet diameter that separates activated droplets from non-activated hydrated particles

Particles with a critical supersaturation above the effective peak supersaturation in the fog will remain in stable equilibrium and their size remains restricted to their stable equilibrium diameter at the ambient RH ($\sim 100\%$). Particles with a critical supersaturation below the effective peak supersaturation will be activated to droplets and keep growing until their water uptake pulls the ambient RH down to 100 %. This will lead to a size separation between the non-activated but hydrated particles and the activated fog droplets, given a sufficient amount of excess water vapour to substantially grow the fog droplets. The resulting minimum in the ambient number size distribution between the modes of the non-activated but hydrated particles and the activated fog droplets approximately represents the size of the particles at the activation threshold, hereafter referred to as $D^{\text{wet}}_{\text{thres}}$. For most fog events no distinct minimum was detected in the number size distribution most probably due to limited growth of the few activated fog droplets. Therefore the surface size distribution of the aerosol was instead used to determine $D^{\text{wet}}_{\text{thres}}$ (see Fig. 2a). In practice this was achieved by fitting a bimodal lognormal distribution to the wet surface size distribution obtained by merging the SMPS and WELAS measurements (see Sect. 3.3). This approach of determining $D^{\text{wet}}_{\text{thres}}$ is essentially equivalent to the method by Elias et al. (2014), except that they used the volume size distribution, which results in slightly larger threshold diameters as will be shown below.

The threshold diameter $D^{\text{wet}}_{\text{thres}}$, which represents the equilibrium diameter at RH = 100 %, was then recalculated to the corresponding dry particle diameter using κ-Köhler theory (Petters and Kreidenweis, 2007, see also Sect. 3.2) and a kappa value

Title Page

Abstract | Introduction

Conclusions | References

Tables | Figures

◀ | ▶|

◀ | ▶

Back | Close

Full Screen / Esc

Printer-friendly Version

Interactive Discussion

of 0.14 (this is the reverse calculation of what is described in Sect. 3.3). The threshold diameter $D_{\text{thres}}^{\text{wet}}$ is considered to be slightly biased high, due to the D^2 weighting of the surface size distribution, and thus the corresponding dry size is considered to represent an upper estimate for the dry activation threshold diameter $D_{\text{act}}^{\text{upper}}$.

3.6 Retrieving the dry activation diameter from the interstitial and total particle size distributions

In the presence of a cloud, the dry activation threshold diameter (D_{act}) can be experimentally determined from the measured dry interstitial and total number size distributions via calculating the activated fraction (AF) of the dry particles with a diameter D^{dry} (see Fig. 3). AF was calculated as follows (Verheggen et al., 2007):

$$\text{AF}(D^{\text{dry}}) = \frac{\frac{\text{d}N_{\text{tot}}}{\text{dlog}D^{\text{dry}}}(D^{\text{dry}}) - \frac{\text{d}N_{\text{int}}}{\text{dlog}D^{\text{dry}}}(D^{\text{dry}})}{\frac{\text{d}N_{\text{tot}}}{\text{dlog}D^{\text{dry}}}(D^{\text{dry}})} \tag{3}$$

where $\frac{\text{d}N_x}{\text{dlog}D^{\text{dry}}}(D^{\text{dry}})$ is the value of the number size distribution at diameter D^{dry} and behind inlet x. The diameter, $D_{\text{act}}^{\text{lower}}$, at which 50 % of the particles of this size were activated, i.e. $\text{AF}(D_{\text{act}}^{\text{lower}}) = 0.5$, provides a lower estimate for the dry activation diameter in the observed fog. It is a lower estimate for the true activation diameter because the largest non-activated particles were sometimes also removed by the interstitial inlet for the setup applied in this study, as further discussed in Sect. 4.2.

3.7 Retrieval of the effective peak supersaturation

Combining D_{act} with the particle hygroscopicity, obtained from the simultaneous CCNC measurements, makes it possible to infer the effective peak supersaturation of the cloud (SS_{peak}) using the κ-Köhler theory (Petters and Kreidenweis, 2007). A detailed description of this procedure can be found in Hammer et al. (2014).

The measured D_{act} and κ are used as input for Eq. (1) to infer the effective peak supersaturation. Thereby it is assumed that the activation occurred at the same temperature as measured 2 m above ground. The theoretical critical supersaturation corresponding to these values, which we define as SS_{peak} of the cloud, is then obtained

5   with the κ-Köhler theory (Sect. 3.2).

The hygroscopicity parameter κ, corresponding to a pair of D^{dry} and SS_{crit} is obtained by numerically solving the SS_{crit}–D^{dry}–κ–relationship for κ. This is used to infer the κ value from the CCNC and SMPS measurements, following the approach by Jurányi et al. (2011).

10   Since two different methods for retrieving D_{act} were addressed in Sect. 3.5 and 3.6, two different SS_{peak} were retrieved: using D^{upper}_{act} and D^{lower}_{act} provides a lower and upper estimate for SS_{peak}, respectively (subsequently referred to as SS^{lower}_{peak} and SS^{upper}_{peak}).

The experimental uncertainty for SS^{upper}_{peak} was estimated using the uncertainties described in Table 1. The variability (25th/75th percentiles) of the κ–D^{dry}–relationship

15   from the time-resolved CCN measurements and the uncertainty from the temperature sensor was used as an estimate for the uncertainty of $\kappa(D_{act})$ (see Sect. 4.1 for further discussion). Applying these uncertainties for the retrieval of SS_{peak}, a relative uncertainty of about 48 % (i.e., ca. one standard deviation) was estimated for SS^{upper}_{peak}.

The uncertainty of SS^{lower}_{peak} is dominated by the uncertainty of D^{wet}_{thres} inferred from the

20   WELAS measurement. Rosati et al. (2014) reported a sizing uncertainty of 15 % for the WELAS instrument, which translated to a relative uncertainty for SS^{lower}_{peak} of about 18 %. The uncertainties of the temperature and κ values have a negligible influence on the overall uncertainty of SS^{lower}_{peak} ($< 3\%$), because in this approach the κ-Köhler theory is essentially just used to extrapolate the dry activation diameter, D^{upper}_{act}, over a very

25   small change in RH and droplet diameter.

Discussion Paper | Discussion Paper | Discussion Paper | Discussion Paper

4   Results and discussion

During the ParisFog 2012/13 campaign 17 developed fog events were detected at the SIRTA site. Table 2 lists all fog events with the corresponding fog type, cut-off diameter at the interstitial inlet and median liquid water content (LWC). The next nine columns show the median effective peak supersaturations (SS_{peak}; lower and upper estimate), median dry activation diameter (D_{act}; lower and upper estimate), median threshold diameter (D_{thres}^{wet}), the scattering coefficients for the modes of hydrated particles ($b_{s, hyd}$) and the activated droplets up to a diameter of 10 µm ($b_{s, drop}$), the fractional contribution of the non-activated but hydrated particles to light scattering of $b_{s, hyd}$ to ($b_{s, hyd} + b_{s, drop}$), and particle extinction coefficient (pec) that are discussed in Sect. 4.2 and 4.3. Seven fog events of the type STL and seven fog events of the type RAD were detected. One fog event of the type PREC was detected, however, neither the SMPS nor the WELAS measured the latter fog type, therefore no results about this event are presented.

Figure 4 gives an overview of the most important meteorological parameters, the fog presence and type (in different color bars), and the total particle number concentration during the campaign. The temperature slightly decreases from the beginning of the campaign towards the end with a minimum value of −6 °C and a maximum value of 23 °C (Fig. 4a). The wind speed at the site was rather moderate during the whole campaign ranging from 0 to 11.3 m s^{-1} (Fig. 4a). There is a high frequency of wind coming from the northeast and thus polluted air from the Paris metropolitan area is transported to the site (Haeffelin et al., 2005). In Fig. 4b, the total particle number concentration is depicted and shows this rather high pollution coming together with northeastern wind directions from Paris. Maximum values of 12 800 cm^{-3} and a median value of 2800 cm^{-3} in the total particle number concentration were encountered. However, the studies of Crippa et al. (2013a) found at the same site that a major part of the fine particulate matter in Paris is contributed by the regional background rather than by local pollution. Thus, the higher pollution with northeastern wind directions

measured at the SIRTA site may be attributed to more continental influence compared to the cleaner western sector, but also to the local influence of road traffic and wood burning emissions (Crippa et al., 2013b, as will be further discussed in Sect. 4.1).

Figure 4c presents the visibility on a log-scale with the threshold at 1 km (dotted line) defining developed fog. Events when the visibility decreased to values between 1 and 5 km are defined as mist or quasi-fog. Such events were investigated at the SIRTA in detail (Elias et al., 2009; Haeffelin et al., 2013). During developed fog, the visibility dropped below 1 km and reached a minimum value of 107 m (1 h average). In earlier campaigns minimum values down to ∼ 50 m were observed at the SIRTA site (Haeffelin et al., 2010). During ParisFog 2012/13 median values of 244 m and 211 m were observed for RAD and STL events, respectively.

4.1 Particle hygroscopic properties during ParisFog 2012/13

The hygroscopicity of aerosol particles is relevant for many atmospheric processes; it can be described with the hygroscopicity parameter κ (Sect. 3.2), which is in required in this study to infer the SS_{peak} from the observed activation diameters. The hygroscopicity parameter as a function of particle dry size, $\kappa(D^{dry})$, was determined from simultaneous total polydisperse CCN number concentration and aerosol size distribution measurements, following the approach described in Jurányi et al. (2011) and Hammer et al. (2014). While total aerosol size distributions are available for the whole period, there are some gaps of the measurement period for the CCN measurements. Therefore, median data of $\kappa(D_{act,CCNC})$ were used to infer SS_{peak} for all the fog events of ParisFog 2012/13.

Figure 5 shows the median κ values observed during ParisFog 2012/13. The median κ value decreased from 0.17 at $D_{dry} = 69$ nm to 0.09 at $D_{dry} = 295$ nm and then increased to 0.19 at 330 nm. The abrupt change between 295 and 330 nm is unreasonable and may be attributed to increased experimental uncertainty of CCN measurements at very low SS. For the Köhler theory calculations in this study we have chosen

a fixed κ value of 0.14 which represents a mean value across the size range from 205 to 330 nm, which is closest to the activation threshold diameter. The κ-values observed in this study are very close to the previously reported winter-time values for the same site (Jurányi et al., 2013; κ = 0.08–0.24 for D_{dry} = 50–177 nm) as well as Paris city centre (Kamilli et al., 2014); κ = 0.17 for D_{dry} = 285 nm). The κ values reported for Paris are substantially lower than the observed and modeled average value of $\kappa \approx 0.3$ for continental sites (Andreae and Rosenfeld, 2008; Pringle et al., 2010). This low κ value is most likely due to the local influence of non- or less-hygroscopic road traffic and residential wood burning emission (Crippa et al., 2013b) which lowers the mean hygroscopicity of the aerosol substantially (Baltensperger et al., 2002; Laborde et al., 2013).

The variability in the κ value over the whole period of ParisFog 2012/13 is indicated by the shaded area between the 25th and 75th percentiles of all data during the three months in Fig. 5. The variability in time in the values is fairly small, particularly between diameters of about 100 nm and 250 nm. At larger particle diameters (250 nm to 350 nm the range between the 25th and 75th percentile increases significantly). This low variability and the fact that SS$_{peak}$ is insignificantly sensitive to κ, permit the use of averaged κ values instead of time-resolved kappa-values derived from simultaneous CCN measurements.

4.2 Observed fog activation properties

For measuring the interstitial aerosols a size cut-off of 1 or 2 µm was used during the campaign (see Sect. 2.2). In another fog-campaign performed in the Po Valley, Italy, a size cut-off of 5 µm was used to distinguish the interstitial from the activated particles (Noone et al., 1992a). Thus, it is important to know which ambient threshold diameter separates the activated fog droplets from the non-activated, but hydrated, particles. In non-fog cloud types, the cooling rates experienced by the air parcel are generally larger than in the case of fog. Therefore the activated droplets experience larger water fluxes resulting in larger growth rates such that the two modes of hydrated

Title Page

Abstract | Introduction

Conclusions | References

Tables | Figures

|◀ | ▶|

◀ | ▶

Back | Close

Full Screen / Esc

Printer-friendly Version

Interactive Discussion

aerosols and activated droplets are much more distinct in diameter for clouds (e.g. at the Jungfraujoch, Switzerland, Henning et al., 2002, or for marine stratus clouds, Baltic Sea, Ditas et al., 2012) than observed in fog, as we will see in the following.

Figure 6a shows the ambient aerosol number size distribution and Fig. 6b the normalized ambient surface size distribution for the fog event F7 detected on 4 November 2012. The aerosol size distribution at ambient RH was obtained by complementing the direct WELAS measurement (for diameters larger than 1.4 µm) with the SMPS measurement of the total aerosol dry size distribution recalculated to RH = 100 % (for the diameter range smaller than 1.4 µm, as detailed in Sect. 3.3). Droplets with diameters larger than ∼ 2 µm are only observed at times with developed fog, i.e. when the visibility is below the threshold value of ∼ 1 km. This suggests that these large droplets represent activated fog droplets, while droplets with diameters <∼2 µm are non-activated but hydrated aerosol particles. The activated fog droplets appear as a distinct mode in the normalized surface size distribution (Fig. 6a). The minimum in the surface size distribution below the fog droplet mode, shown with orange markers in Fig. 6b, is considered to be an estimate of the threshold diameter, $D_{\text{thres}}^{\text{wet}}$, for fog droplet activation, as detailed in Sect. 3.5.

The cut-off diameter of 1 µm applied at the interstitial inlet for the example in Fig. 6 is always clearly below the wet activation threshold diameter. Thus, a significant fraction of the non-activated but hydrated particles are removed from the interstitial inlet, in addition to the fog droplets which are supposed to be removed. In those cases the dry activation diameter (D_{act}), as explained in Sect. 3.6, reflects the dry size corresponding to the hydrated particles with an equilibrium size at ambient RH that is equal to the cut-off of the interstitial inlet. Thus, the inferred D_{act} is a lower estimate for the dry activation threshold diameter and is called $D_{\text{act}}^{\text{lower}}$. The bias introduced by this artifact is more significant the lower the cut-off of the interstitial inlet is. Thus, the results obtained from measurements with the 2 µm-cut-off are expected to be closer to the true value than those obtained with the 1 µm-cut-off. This is illustrated with the ambient aerosol number and surface size distributions observed during fog event F11 (Fig. 7a and b),

Title Page

Abstract | Introduction

Conclusions | References

Tables | Figures

◄ | ►

◄ | ►

Back | Close

Full Screen / Esc

Printer-friendly Version

Interactive Discussion

when a 2 μm-cut-off was applied at the interstitial inlet. In this case, the wet activation threshold diameter is closer to the inlet cut-off and thus the bias in the retrieved D_{act}^{lower} is expected to be small.

Figure 6c shows the dry activation diameters D_{act}^{upper} and D_{act}^{lower} inferred from the wet activation threshold diameter and the interstitial/total dry size distribution measurements for fog event F11, respectively (see Sects. 3.5 and 3.6 for the methodology). The difference between D_{act}^{upper} and D_{act}^{lower} is small when the wet activation threshold diameter is around the cut-off of the interstitial inlet and larger at other times.

The estimate of D_{act} combined with the particle hygroscopicity from CCN measurements are the basis to infer the effective peak supersaturation (SS_{peak}) of fog according to the methodology addressed in Sect. 3.7. The CCN activation behavior of the particles, required to infer SS_{peak} with Köhler theory, was taken from the averaged CCN measurements (Fig. 5). Figure 7d shows the lower and upper limit estimates of the effective peak supersaturation, SS_{peak}^{lower} and SS_{peak}^{upper}, corresponding to the upper and lower limit estimates of the dry activation diameter, D_{act}^{upper} and D_{act}^{lower}, respectively. The results for the fog event F11 indicate a very low supersaturation in the range between ~ 0.016 to 0.113%.

An overview of the results for all fog events observed in this study is shown in Fig. 8, where the visibility range (Fig. 8a), was used to identify the periods with developed fog. Figure 8b shows the time series of the ambient threshold wet diameter, D_{thres}^{wet}, separating the unactivated but hydrated particles and the fog droplets, as determined for all fog events when WELAS data is available. The conditions during the fog droplet formation in the vicinity of the SIRTA site are characterized by considerable variability (see also Table 2). The observed D_{thres}^{wet} values shown in Fig. 8b vary between 1 and 5 μm with a campaign median of 2.6 μm. Elias et al. (2014) reported an average of 4.0 ± 1.1 μm, derived from volume size distributions of developed fogs measured in November 2011. Using the volume size distributions (Elias et al., 2014) instead of surface size distributions (this study) for deriving D_{thres}^{wet} results in slightly higher threshold diameters and therefore their result is in good agreement with the values presented in this study here.

This overestimation of the threshold diameters, due to deriving D_{thres}^{wet} based on volume size distributions, is also the reason why in this study the surface size distribution was used to infer the D_{thres}^{wet} instead of using the volume size distribution.

The upper and lower limit estimates of the dry activation diameter are shown in Fig. 8 and median values for all fog events are provided in Table 2.

The lower estimates for the dry activation diameter, D_{act}^{lower}, are systematically smaller for the fog events F4 to F9, when the 1 µm-cut-off was applied at the interstitial inlet, compared to the results for fog events F1 to F3 and F11 to F15, obtained with the 2 µm-cut-off. This difference in D_{act}^{lower} between the two subsets is artificial and can be attributed to the larger low bias introduced by the 1 µm-cut-off. The fact that the upper limit estimates of the dry activation diameter, D_{act}^{upper}, do not exhibit a systematic differ-ence between the two subsets, excludes a difference in the fog properties as a cause. The true activation diameter is likely between D_{act}^{upper} and D_{act}^{lower} from the measurements with the 2 µm-cut-off.

All fog events feature rather high median D_{act}^{lower} and D_{act}^{upper} indicating that only a small fraction at the upper end of the particle size distribution is able to activate to fog droplets. The range of dry activation diameters observed in this study overlaps with the range of typical D_{act} values reported in other fog studies (~ 300 to ~ 500 nm; e.g. Noone et al., 1992a; Ming and Russell, 2004). However, the dry activation diameters observed in the fog are considerably larger than those observed and/or inferred within stratus or cumulus clouds (e.g. Ditas et al., 2012; Hammer et al., 2014; Hudson and Rogers, 1986; Krueger et al., 2013; McFiggans et al., 2006) due to the lower SS_{peak} encountered in fog.

The effective peak supersaturations determined for all fog events during ParisFog 2012/13 are shown in Fig. 8d. For the upper estimate, the results from events F11–F15 (2 µm cut-off) are expected to be closer to the true value for the reasons ex-plained above. The effective peak supersaturation is always very low with limiting val-ues between 0.016 % and 0.113 %. Differences in the observed SS_{peak} values between different fog events are of similar magnitude as the accuracy. Nevertheless, these

Title Page

Abstract | Introduction

Conclusions | References

Tables | Figures

◄ | ►

◄ | ►

Back | Close

Full Screen / Esc

differences reflect true differences of the fog properties, as the small point-to-point variability of adjacent data points indicates a relatively high precision. The median effective peak supersaturation falls between $SS_{peak}^{lower} \approx 0.03\%$ and $SS_{peak}^{upper} \approx 0.05\%$ (see Table 2). The variability of the effective peak supersaturation values is shown in Fig. 9. Half of the data points fall between 0.02 % (25th percentile of SS_{peak}^{lower}; 2 µm data only) and 0.06 % (75th percentile of SS_{peak}^{upper}), while the respective 10th and 90th percentile values are 0.017 % and 0.1 %. These values observed during ParisFog 2012/2013 are within the range of previous literature reports of measured and modeled peak supersaturations in fog ($SS_{peak} < \sim 0.1\%$; e.g. Meng and Seinfeld, 1994; Pandis and Seinfeld, 1989).

4.3 Contribution of hydrated particles and fog droplets to light scattering

Visibility is dramatically reduced during the presence of fog. It can decrease from a few kilometers to a few meters within minutes (as occurred for example on 30 November 2012). However, it was observed that only a few of the larger particles usually are able to activate to fog droplets (10 to 150 cm^{-3}; Burnet et al., 2012; Elias et al., 2014).

Elias et al. (2014) showed for earlier campaigns at the same site that hydrated aerosols have a non-negligible contribution to visibility reduction during fog events (500 to 3500 Mm^{-1}). In order to assess the contributions of the hydrated and activated aerosol to the light scattering, they computed the light scattering coefficient b_s, as described in Sect. 3.4. For comparison, Fig. 10 shows the averaged b_s size distribution measured by the WELAS instrument and retrieved from the estimated wet size distribution from the SMPS instrument for the present study. Table 2 presents the light scattering coefficient of the hydrated aerosol mode ($b_{s,\,hyd}$):

$$b_{s,\,hyd} = \int_{D_{min}}^{D_{thres}^{wet}} \frac{\mathrm{d}b_s}{\mathrm{dlog}D^{wet}} \mathrm{dlog}D^{wet} \qquad (4)$$

and the light scattering coefficient of the droplet mode ($b_{s,\,drop}$):

$$b_{s,\,drop} = \int_{D_{thres}^{wet}}^{D_{max}} \frac{\mathrm{d}b_s}{\mathrm{d}\log D^{wet}} \, dlog D^{wet}. \tag{5}$$

D_{max} is the largest diameter covered by the WELAS measurement of the ambient size distribution. Additionally, the fractional contribution, $\frac{b_{s,\,hyd}}{(b_{s,\,drop}+b_{s,\,hyd})}$, of the hydrated particles mode to the total light scattering coefficient of all particles and droplets is reported. This fraction ranges from 49 up to 93 % with a median of 69 % (see Table 2). The studies of Burnet et al. (2012) and Elias et al. (2014) showed that WELAS measurements alone are not able to reproduce the light scattering of the larger fog droplets (only droplets up to a size range of $\sim 10\,\mu m$ can be detected with a WELAS). In order to obtain an estimate of the total light scattering of all particles including all fog droplets, the WELAS data would need to be complemented with a fog droplet probe. Another method is to calculate the particle extinction coeffcient (pec) from the visibilimeter data using the Koschmieder equation (Koschmieder, 1925; Harrison, 2012) as has been done in Elias et al. (2009):

$$pec = \frac{-\ln(C_v)}{visibility} \tag{6}$$

C_v is the visual contrast, which is defined at 5 % for the visibilimeter. The pec is retrieved for a halogen lamp spectrum (in the wavelength range 350–900 nm peaking at 550 nm; spectrum used from www.uvguide.co.uk, which is similar to the visible part of the solar spectrum) and is listed in Table 2. During most of the fog events the pec values are higher than ($b_{s,\,hyd} + b_{s,\,drop}$), which can to some extent be attributed to the undetected largest fog droplets. Thus, the fraction $\frac{b_{s,\,hyd}}{b_{s,\,drop}+b_{s,\,hyd}}$ is overestimated, however, since the difference between pec and ($b_{s,\,drop} + b_{s,\,hyd}$) is only moderate it can still be

Particle activation properties in fog

E. Hammer et al.

Title Page

Abstract | Introduction

Conclusions | References

Tables | Figures

|◄ | ►|

◄ | ►

Back | Close

Full Screen / Esc

Printer-friendly Version

Interactive Discussion

concluded that the hydrated but non-activated particles give a significant contribution to the visibility reduction.

5   Conclusions

During the ParisFog 2012/13 field campaign, performed at the semi-urban site SIRTA in Palaiseau, close to Paris, 17 developed fog events were observed and examined regarding their aerosol-to-fog droplet activation properties. Aerosol and droplet size distributions were obtained at ambient relative humidity. The activated fraction of the particles was acquired using total and interstitial particle dry size distribution measurements. CCN number concentrations were measured at different SS to obtain particle hygroscopicity.

The hygroscopicity parameter, κ, was calculated for the whole campaign and values in the range of measured particle diameters were found between 0.06 and 0.27, and centered at 0.14. These values are in the same range as observed in an earlier study performed at SIRTA during Megapoli 2010. However, these values are at the lower end of values modeled for continental aerosols (e.g. Andreae and Rosenfeld, 2008). These rather low values likely indicate subtantial influence of local road traffic and wood burning emissions (Crippa et al., 2013b), which are known to be only weakly hygroscopic (Baltensperger et al., 2002; Laborde et al., 2013).

Two alternative approaches were applied to investigate the fog droplet activation process. The wet activation threshold diameter, separating the activated fog droplets from the non-activated but hydrated particles, was found to be around 2.6 μm. The median dry activation cut-off diameter was estimated to fall between 364 and 450 nm. This implies a median peak supersaturation between 0.03 % and 0.05 % for ParisFog 2012/2013, which is in good agreement with literature values.

During all 17 fog events, hydrated particles contributed 69 % to the light scattering (although this value is slightly overestimated due to under-counting of droplets).

This study revealed a very weak separation between the activated fog droplets and the non-activated but hydrated particles. This makes it difficult to use an interstitial inlet for separating the non-activated particles from the activated fog droplets. Thus, great care has to be taken to choose the ideal inlet cut-off, possibly variable in time, in order to avoid or minimize biases that can be introduced by removing too many small or too few large particles in the inlet, if the cut-off falls into one of the two modes rather than in between them.

References

Allan, J. D., Baumgardner, D., Raga, G. B., Mayol-Bracero, O. L., Morales-García, F., García-García, F., Montero-Martínez, G., Borrmann, S., Schneider, J., Mertes, S., Walter, S., Gysel, M., Dusek, U., Frank, G. P., and Krämer, M.: Clouds and aerosols in Puerto Rico – a new evaluation, Atmos. Chem. Phys., 8, 1293–1309, doi:10.5194/acp-8-1293-2008, 2008. 9505

Andreae, M. O. and Rosenfeld, D.: Aerosol-cloud-precipitation interactions, Part 1. The nature and sources of cloud-active aerosols, Earth-Sci. Rev., 89, 13–41, doi:10.1016/j.earscirev.2008.03.001, 2008. 9491, 9497

Baltensperger, U., Streit, N., Weingartner, E., Nyeki, S., Prévôt, A. S. H., Van Dingenen, R., Virkkula, A., Putaud, J.-P., Even, A., ten Brink, H., Blatter, A., Neftel, A., and Gäggeler, H. W.: Urban and rural aerosol characterization of summer smog events during the PIPAPO field campaign in Milan, Italy, J. Geophys. Res.-Atmos., 107, 2156–2202, doi:10.1029/2001JD001292, 2002. 9491, 9497

Bergot, T.: Quality assessment of the Cobel-Isba numerical forecast system of fog and low clouds, Pure Appl. Geophys., 164, 1265–1282, doi:10.1007/s00024-007-0218-3, 2007. 9478

Bott, A., Sievers, U., and Zdunkowski, W.: A radiation fog model with a detailed treatment of the interaction between radiative-transfer and fog microphysics, J. Atmos. Sci., 47, 2153–2166, doi:10.1175/1520-0469(1990)047<2153:ARFMWA>2.0.CO;2, 1990. 9479

Burnet, F., Gomes, L., Haeffelin, M., Dupont, J., and Elias, T.: Analysis of the microphysical structures of fog during the ParisFog project, in: Proceedings of the 16th international conference of clouds and precipitation (ICCP), Leipzig, Germany, 30 July–3 August, 582, 2012. 9483, 9495, 9496

Crippa, M., DeCarlo, P. F., Slowik, J. G., Mohr, C., Heringa, M. F., Chirico, R., Poulain, L., Freutel, F., Sciare, J., Cozic, J., Di Marco, C. F., Elsasser, M., Nicolas, J. B., Marchand, N., Abidi, E., Wiedensohler, A., Drewnick, F., Schneider, J., Borrmann, S., Nemitz, E., Zimmermann, R., Jaffrezo, J.-L., Prévôt, A. S. H., and Baltensperger, U.: Wintertime aerosol chemical composition and source apportionment of the organic fraction in the metropolitan area of Paris, Atmos. Chem. Phys., 13, 961–981, doi:10.5194/acp-13-961-2013, 2013a. 9489

Crippa, M., El Haddad, I., Slowik, J. G., DeCarlo, P. F., Mohr, C., Heringa, M. F., Chirico, R., Marchand, N., Sciare, J., Baltensperger, U., and Prevot, A. S. H.: Identification of marine and continental aerosol sources in Paris using high resolution aerosol mass spectrometry, J. Geophys. Res.-Atmos., 118, 1950–1963, doi:10.1002/jgrd.50151, 2013b. 9490, 9491, 9497

David, N., Alpert, P., and Messer, H.: The potential of cellular network infrastructures for sudden rainfall monitoring in dry climate regions, Atmos. Res., 131, 13–21, doi:10.1016/j.atmosres.2013.01.004, 2013. 9478

Ditas, F., Shaw, R. A., Siebert, H., Simmel, M., Wehner, B., and Wiedensohler, A.: Aerosols-cloud microphysics-thermodynamics-turbulence: evaluating supersaturation in a marine stratocumulus cloud, Atmos. Chem. Phys., 12, 2459–2468, doi:10.5194/acp-12-2459-2012, 2012. 9492, 9494

Dupont, J.-C., Haeffelin, M., Protat, A., Bouniol, D., Boyouk, N., and Morille, Y.: Stratus – fog formation and dissipation: a 6-day case study, Bound.-Lay. Meteorol., 143, 207–225, doi:10.1007/s10546-012-9699-4, 2012. 9483

Duynkerke, P. G.: Radiation fog: a comparison of model simulation with detailed observations, Mon. Weather Rev., 119, 324–341, doi:10.1175/1520-0493(1991)119<0324:RFACOM>2.0.CO;2, 1991. 9478

Title Page

Abstract | Introduction

Conclusions | References

Tables | Figures

|◄ | ►|

◄ | ►

Back | Close

Full Screen / Esc

Printer-friendly Version

Interactive Discussion

Elias, T., Haeffelin, M., Drobinski, P., Gomes, L., Rangognio, J., Bergot, T., Chazette, P., Raut, J.-C., and Colomb, M.: Particulate contribution to extinction of visible radiation: pollution, haze, and fog, Atmos. Res., 92, 443–454, doi:10.1016/j.atmosres.2009.01.006, 2009. 9478, 9479, 9490, 9496, 9505

Elias, T., Dupont, J.-C., Burnet, F., Haeffelin, M., Jolivet, D., and Hammer, E.: Aerosols affecting the radiative budget during the fog life cycle: microphysical properties and extinction coefficient, Atmos. Res., in review, 2014. 9483, 9486, 9493, 9495, 9496

Facchini, M. C., Fuzzi, S., Lind, J. A., Fierlinger-Oberlinninger, H., Kalina, M., Puxbaum, H., Winiwarter, W., Arends, B. G., Wobrock, W., Jaeschke, W., Berner, A., and Kruisz, C.: Phase-partitioning and chemical reactions of low molecular weight organic compounds in fog, Tellus B, 44, 533–544, doi:10.1034/j.1600-0889.1992.t01-3-00007.x, 1992. 9478

Fuzzi, S., Facchini, M. C., Orsi, G., and Ferri, D.: Seasonal trend of fog water chemical composition in the Po Valley, Environ. Pollut., 75, 75–80, doi:10.1016/0269-7491(92)90059-J, 1992. 9478

Gerber, H.: Supersaturation and droplet spectral evolution in fog, J. Atmos. Sci., 48, 2569–2588, doi:10.1175/1520-0469(1991)048<2569:Sadsei>2.0.Co;2, 1991. 9482

Guedalia, D. and Bergot, T.: Numerical forecasting of radiation fog, Part II: A comparison of model simulation with several observed fog events, Mon. Weather Rev., 122, 1231–1246, doi:10.1175/1520-0493(1994)122<1231:NFORFP>2.0.CO;2, 1994. 9478

Gultepe, I., Tardif, R., Michaelides, S. C., Cermak, J., Bott, A., Bendix, J., Müller, M. D., Pagowski, M., Hansen, B., Ellrod, G., Jacobs, W., Toth, G., and Cober, S. G.: Fog research: a review of past achievements and future perspectives, Pure Appl. Geophys., 164, 1121–1159, doi:10.1007/s00024-007-0211-x, 2007. 9478, 9479

Haeffelin, M., Barthès, L., Bock, O., Boitel, C., Bony, S., Bouniol, D., Chepfer, H., Chiriaco, M., Cuesta, J., Delanoë, J., Drobinski, P., Dufresne, J.-L., Flamant, C., Grall, M., Hodzic, A., Hourdin, F., Lapouge, F., Lemaître, Y., Mathieu, A., Morille, Y., Naud, C., Noël, V., O'Hirok, W., Pelon, J., Pietras, C., Protat, A., Romand, B., Scialom, G., and Vautard, R.: SIRTA, a ground-based atmospheric observatory for cloud and aerosol research, Ann. Geophys., 23, 253–275, doi:10.5194/angeo-23-253-2005, 2005. 9480, 9489

Haeffelin, M., Bergot, T., Elias, T., Tardif, R., Carrer, D., Chazette, P., Colomb, M., Drobinski, P., Dupont, E., Dupont, J. C., Gomes, L., Musson-Genon, L., Pietras, C., Plana-Fattori, A., Protat, A., Rangognio, J., Raut, J. C., Remy, S., Richard, D., Sciare, J., and Zhang, X.: Paris-

Title Page

Abstract | Introduction

Conclusions | References

Tables | Figures

|◄ | ►|

◄ | ►

Back | Close

Full Screen / Esc

Printer-friendly Version

Interactive Discussion

fog shedding new light on fog physical processes, B. Am. Meteorol. Soc., 91, 767–783, doi:10.1175/2009BAMS2671.1, 2010. 9478, 9480, 9483, 9490

Haeffelin, M., Dupont, J.-C., Boyouk, N., Baumgardner, D., Gomes, L., Roberts, G., and Elias, T.: A Comparative Study of Radiation Fog and Quasi-Fog Formation Processes During the ParisFog Field Experiment 2007, Pure Appl. Geophys., 170, 2283–2303, doi:10.1007/s00024-013-0672-z, 2013. 9490

Hammer, E., Bukowiecki, N., Gysel, M., Jurányi, Z., Hoyle, C. R., Vogt, R., Baltensperger, U., and Weingartner, E.: Investigation of the effective peak supersaturation for liquid-phase clouds at the high-alpine site Jungfraujoch, Switzerland (3580 m a.s.l.), Atmos. Chem. Phys., 14, 1123–1139, doi:10.5194/acp-14-1123-2014, 2014. 9479, 9487, 9490, 9494

Harrison, R.: Aerosol-induced correlation between visibility and atmospheric electricity, J. Aerosol Sci., 52, 121–126, doi:10.1016/j.jaerosci.2012.04.011, 2012. 9496

Heim, M., Mullins, B. J., Umhauer, H., and Kasper, G.: Performance evaluation of three optical particle counters with an efficient "multimodal" calibration method, J. Aerosol Sci., 39, 1019–1031, doi:10.1016/j.jaerosci.2008.07.006, 2008. 9483

Heintzenberg, J.: The Po Valley Fog Experiment 1989 – what have we learned, where do we go from here?, Tellus B, 44, 443–447, doi:10.1034/j.1600-0889.1991.t01-3-00002.x-i1, 1992. 9478

Henning, S., Weingartner, E., Schmidt, S., Wendisch, M., Gaggeler, H. W., and Baltensperger, U.: Size-dependent aerosol activation at the high-alpine site Jungfraujoch (3580 m a.s.l.), Tellus B, 54, 82–95, doi:10.1034/j.1600-0889.2002.00299.x, 2002. 9492

Hudson, J. G. and Rogers, C. F.: Relationship between critical supersaturation and cloud droplet size: implications for cloud mixing processes, J. Atmos. Sci., 43, 2341–2359, doi:10.1175/1520-0469(1986)043<2341:RBCSAC>2.0.CO;2, 1986. 9494

Hupfer, P., Kuttler, W., and Chmielewski, F.-M.: Witterung und Klima: eine Einfuehrung in die Meteorologie und Klimatologie, Springer, Germany, 2005. 9484

Jurányi, Z., Gysel, M., Weingartner, E., Bukowiecki, N., Kammermann, L., and Baltensperger, U.: A 17 month climatology of the cloud condensation nuclei number concentration at the high alpine site Jungfraujoch, J. Geophys. Res.-Atmos., 116, 2156–2202, doi:10.1029/2010JD015199, 2011. 9488, 9490

Jurányi, Z., Tritscher, T., Gysel, M., Laborde, M., Gomes, L., Roberts, G., Baltensperger, U., and Weingartner, E.: Hygroscopic mixing state of urban aerosol derived from size-resolved

cloud condensation nuclei measurements during the MEGAPOLI campaign in Paris, Atmos. Chem. Phys., 13, 6431–6446, doi:10.5194/acp-13-6431-2013, 2013. 9491

Kamilli, K. A., Poulain, L., Held, A., Nowak, A., Birmili, W., and Wiedensohler, A.: Hygroscopic properties of the Paris urban aerosol in relation to its chemical composition, Atmos. Chem. Phys., 14, 737–749, doi:10.5194/acp-14-737-2014, 2014. 9491

Kim, C. and Yum, S.: A numerical study of sea-fog formation over cold sea surface using a one-dimensional turbulence model coupled with the weather research and forecasting model, Bound.-Lay. Meteorol., 143, 481–505, doi:10.1007/s10546-012-9706-9, 2012. 9479

Köhler, H.: The nucleus in and the growth of hygroscopic droplets, T. Faraday Soc., 32, 1152–1161, 1936. 9484

Koschmieder, H.: Theorie der horizontalen Sichtweite, Beiträge Physicae Freiberger Atmosphere, 12, 171–181, 1925. 9496

Krüger, M. L., Mertes, S., Klimach, T., Cheng, Y., Su, H., Schneider, J., Andreae, M. O., Pöschl, U., and Rose, D.: Assessment of cloud supersaturation by aerosol particle and cloud condensation nuclei (CCN) measurements, Atmos. Meas. Tech. Discuss., 6, 10021–10056, doi:10.5194/amtd-6-10021-2013, 2013. 9494

Laborde, M., Crippa, M., Tritscher, T., Jurányi, Z., Decarlo, P. F., Temime-Roussel, B., Marchand, N., Eckhardt, S., Stohl, A., Baltensperger, U., Prévôt, A. S. H., Weingartner, E., and Gysel, M.: Black carbon physical properties and mixing state in the European megacity Paris, Atmos. Chem. Phys., 13, 5831–5856, doi:10.5194/acp-13-5831-2013, 2013. 9491, 9497

Maier, F., Bendix, J., and Thies, B.: Development and application of a method for the objective differentiation of fog life cycle phases, Tellus B, 65, doi:10.3402/tellusb.v65i0.19971, 2013. 9478

McFiggans, G., Artaxo, P., Baltensperger, U., Coe, H., Facchini, M. C., Feingold, G., Fuzzi, S., Gysel, M., Laaksonen, A., Lohmann, U., Mentel, T. F., Murphy, D. M., O'Dowd, C. D., Snider, J. R., and Weingartner, E.: The effect of physical and chemical aerosol properties on warm cloud droplet activation, Atmos. Chem. Phys., 6, 2593–2649, doi:10.5194/acp-6-2593-2006, 2006. 9479, 9494

Meng, Z. and Seinfeld, J. H.: On the source of the submicrometer droplet mode of urban and regional aerosols, Aerosol Sci. Tech., 20, 253–265, doi:10.1080/02786829408959681, 1994. 9495

Meyer, M. B., Lala, G. G., and Jiusto, J. E.: Fog-82: a cooperative field study of radiation fog, B. Am. Meteorol. Soc., 67, 825–832, doi:10.1175/1520-0477(1986)067<0825:FACFSO>2.0.CO;2, 1986. 9478

Ming, Y. and Russell, L. M.: Organic aerosol effects on fog droplet spectra, J. Geophys. Res.-Atmos., 109, 2156–2202, doi:10.1029/2003JD004427, 2004. 9494

Noone, K. J., Ogren, J. A., Hallberg, A., Hansson, H. C., Wiedensohler, A., and Swietlicki, E.: A statistical examination of the chemical differences between interstitial and scavenged aerosol, Tellus B, 44, 581–592, doi:10.1034/j.1600-0889.1992.t01-1-00011.x, 1992a. 9491, 9494

Noone, K. J., Ogren, J. A., Hallberg, A., Heintzenberg, J., Strom, J., Hansson, H. C., Svenningsson, B., Wiedensohler, A., Fuzzi, S., Facchini, M. C., Arends, B. G., and Berner, A.: Changes in aerosol size and phase distributions due to physical and chemical processes in fog, Tellus B, 44, 489–504, doi:10.1034/j.1600-0889.1992.t01-4-00004.x, 1992b. 9478

Pandis, S. N. and Seinfeld, J. H.: Mathematical-modeling of acid deposition due to radiation fog, J. Geophys. Res.-Atmos., 94, 12911–12923, doi:10.1029/JD094iD10p12911, 1989. 9495

Petters, M. D. and Kreidenweis, S. M.: A single parameter representation of hygroscopic growth and cloud condensation nucleus activity, Atmos. Chem. Phys., 7, 1961–1971, doi:10.5194/acp-7-1961-2007, 2007. 9479, 9484, 9485, 9486, 9487

Pringle, K. J., Tost, H., Pozzer, A., Pöschl, U., and Lelieveld, J.: Global distribution of the effective aerosol hygroscopicity parameter for CCN activation, Atmos. Chem. Phys., 10, 5241–5255, doi:10.5194/acp-10-5241-2010, 2010. 9491

Roberts, G. C. and Nenes, A.: A continuous-flow streamwise thermal-gradient CCN chamber for atmospheric measurements, Aerosol Sci. Tech., 39, 206–221, doi:10.1080/027868290913988, 2005. 9482

Rosati, B., Zieger, P., Gysel, M., Baltensperger, U., and Weingartner, E.: The white-light humidified optical particle spectrometer (WHOPS) – a novel airborne system to characterize aerosol hygroscopicity, Atmos. Meas. Tech. Discuss., in preparation, 2014. 9488

Rosenfeld, J.: Cars vs. the weather: a century of progress, Weatherwise, 49, 14–23, doi:10.1080/00431672.1996.9925430, 1996. 9478

Stolaki, S., Pytharoulis, I., and Karacostas, T.: A study of fog characteristics using a coupled WRF-COBEL model over Thessaloniki airport, Greece, Pure Appl. Geophys., 169, 961–981, doi:10.1007/s00024-011-0393-0, 2012. 9479

Title Page

Abstract | Introduction

Conclusions | References

Tables | Figures

◀ | ▶

◀ | ▶

Back | Close

Full Screen / Esc

Printer-friendly Version

Interactive Discussion

Sullivan, R. C., Moore, M. J. K., Petters, M. D., Kreidenweis, S. M., Roberts, G. C., and Prather, K. A.: Effect of chemical mixing state on the hygroscopicity and cloud nucleation properties of calcium mineral dust particles, Atmos. Chem. Phys., 9, 3303–3316, doi:10.5194/acp-9-3303-2009, 2009. 9482

Svenningsson, I. B., Hansson, H. C., Wiedensohler, A., Ogren, J. A., Noone, K. J., and Hallberg, A.: Hygroscopic growth of aerosol-particles in the Po Valley, Tellus B, 44, 556–569, doi:10.1034/j.1600-0889.1992.t01-1-00009.x, 1992. 9478

Tardif, R. and Rasmussen, R. M.: Event-based climatology and typology of fog in the New York City region, J. Appl. Meteorol. Clim., 46, 1141–1168, doi:10.1175/JAM2516.1, 2007. 9478, 9483

Vautard, R., Yiou, P., and van Oldenborgh, G. J.: Decline of fog, mist and haze in Europe over the past 30 years, Nat. Geosci., 2, 115–119, doi:10.1038/ngeo414, 2009. 9478

Verheggen, B., Cozic, J., Weingartner, E., Bower, K., Mertes, S., Connolly, P., Gallagher, M., Flynn, M., Choularton, T., and Baltensperger, U.: Aerosol partitioning between the interstitial and the condensed phase in mixed-phase clouds, J. Geophys. Res.-Atmos., 112, 2156–2202, doi:10.1029/2007JD008714, 2007. 9487

Wiedensohler, A., Birmili, W., Nowak, A., Sonntag, A., Weinhold, K., Merkel, M., Wehner, B., Tuch, T., Pfeifer, S., Fiebig, M., Fjäraa, A. M., Asmi, E., Sellegri, K., Depuy, R., Venzac, H., Villani, P., Laj, P., Aalto, P., Ogren, J. A., Swietlicki, E., Williams, P., Roldin, P., Quincey, P., Hüglin, C., Fierz-Schmidhauser, R., Gysel, M., Weingartner, E., Riccobono, F., Santos, S., Grüning, C., Faloon, K., Beddows, D., Harrison, R., Monahan, C., Jennings, S. G., O'Dowd, C. D., Marinoni, A., Horn, H.-G., Keck, L., Jiang, J., Scheckman, J., McMurry, P. H., Deng, Z., Zhao, C. S., Moerman, M., Henzing, B., de Leeuw, G., Löschau, G., and Bastian, S.: Mobility particle size spectrometers: harmonization of technical standards and data structure to facilitate high quality long-term observations of atmospheric particle number size distributions, Atmos. Meas. Tech., 5, 657–685, doi:10.5194/amt-5-657-2012, 2012. 9505

Zhao, C. F., Klein, S. A., Xie, S. C., Liu, X. H., Boyle, J. S., and Zhang, Y. Y.: Aerosol first indirect effects on non-precipitating low-level liquid cloud properties as simulated by CAM5 at ARM sites, Geophys. Res. Lett., 39, 1944–8007, doi:10.1029/2012gl051213, 2012. 9479

Table 1. Instrumentation deployed during ParisFog 2012/13 that provided data for this study.

Measured parameter(s)	Instrument	Accuracy	Measurement range	Time resolution
dry aerosol number size distribution	Scanning Mobility Particle Sizer (SMPS)	Number conc.: ±20 % (20 < D < 520 nm;) (Wiedensohler et al., 2012)	D = 13–520 nm	6 min
ambient aerosol and droplet number size distribution	Palas Welas-2000 Particle Counter	Number conc.: ±20 % (Elias et al., 2009)	D = 1.4–10 µm[*] (for water spheres)	5 min
Cloud Condensation Nuclei (CCN) number concentration	Continuous flow streamwise thermal gradient CCN chamber	SS: ±10 % Number conc.: ±10 %	SS = 0.05–0.6 %	1 s (20 min/ spectra)
Visibility	Degreanne DF20+ forward scatter sensor	< 5 km: ±10 % 5–20 km: ±15 % > 20 km: ±25 %	5 m–70 km	1 min
Liquid water content (LWC)	Particle Volume Monitor (PVM-100)	±15 % (Allan et al., 2008)	D = 3–50 µm	1 min
Temperature	PT-100 ATDM – MH13	±0.1 K (EdgeTech datasheet)	−100–250 °C	1 min

[*]Size range with a detection efficiency of ∼ 1. The full size range of the instrument is: D = 0.36–42 µm.

Particle activation properties in fog

E. Hammer et al.

Title Page

Abstract | Introduction

Conclusions | References

Tables | Figures

|◄ | ►|

◄ | ►

Back | Close

Full Screen / Esc

Printer-friendly Version

Interactive Discussion

Table 2. Overview of the Fog events measured during ParisFog 2012/13. The three observed fog types are indicated as STL: stratus lowering, RAD: radiation, PREC: precipitation fog. LWC indicates the liquid water content, D_{act} is the dry activation diameter[2], D_{thres}^{wet} is the wet activation threshold diameter[1], $b_{s,hyd}$ is the light scattering of the hydrated but unactivated aerosol mode and $b_{s,drop}$ of the droplet mode, and pec is the total particle extinction coefficient. The campaign median is given for all values on the bottom line.

Fog Number	Start Time [UTC]	End Time [UTC]	Fog type	Cut-off at int. inlet [µm]	Median LWC [mg m^{-3}]	Median SS$_{peak}$ [%] lower[1]	upper[2]	Median D_{act}^{dry} [nm] lower[2]	upper[1]	Median D_{thres}^{wet}[1] [µm]	$b_{s,hyd}$[3] [Mm^{-1}]	$b_{s,drop}$[4] [Mm^{-1}]	$\frac{b_{s,hyd}}{b_{s,drop}+b_{s,hyd}}$ [-]	pec [Mm^{-1}]
F1	10 Oct 2012 02:09	10 Oct 2012 07:45	STL	2	–	–	0.04	408	–	–	–	–	–	8996
F2	11 Oct 2012 01:09	11 Oct 2012 08:33	STL	2	–	–	0.04	361	–	–	–	–	–	25469
F3	14 Oct 2012 02:57	14 Oct 2012 07:21	RAD	2	–	–	0.06	312	–	–	–	–	–	16063
F4	2 Oct 2012 06:21	2 Oct 2012 08:33	STL	1	11	0.01	0.09	277	617	3.9	5320	420	0.93	4630
F5	2 Oct 2012 03:33	2 Oct 2012 07:57	RAD	1	27	0.02	0.09	280	647	4.2	4680	1550	0.75	10080
F6	2 Oct 2012 03:45	2 Oct 2012 05:33	RAD	1	64	0.03	0.11	254	435	2.3	3910	2720	0.59	5350
F7	4 Nov 2012 00:57	4 Nov 2012 05:33	RAD	1	61	0.03	0.11	251	441	2.4	2330	2450	0.49	9030
F8	9 Nov 2012 06:45	9 Nov 2012 11:21	RAD	1	119	0.03	0.11	261	450	2.4	6930	1110	0.86	18000
F9	11 Nov 2012 23:57	12 Nov 2012 09:57	STL	1	37	0.03	0.11	261	451	2.4	3780	2310	0.62	8160
F10	14 Nov 2012 09:33	14 Nov 2012 11:57	RAD	1	62	–	0.11	262	–	–	–	–	–	3860
F11	15 Nov 2012 23:57	16 Nov 2012 15:57	STL	2	114	0.02	0.05	364	535	3.2	7850	3560	0.69	22340
F12	16 Nov 2012 20:33	17 Nov 2012 08:57	STL	2	74	0.04	0.07	302	398	2.0	2610	1810	0.59	13950
F13	20 Nov 2012 20:21	20 Nov 2012 22:45	STL	2	102	0.02	–	–	590	3.7	5570	740	0.88	11280
F14	22 Nov 2012 03:21	22 Nov 2012 08:57	RAD	2	87	0.04	0.05	366	376	1.9	6970	3090	0.69	13150
F15	30 Nov 2012 18:57	1 Dec 2012 02:33	RAD	2	35	0.02	0.04	435	544	3.2	9940	5860	0.63	13140
F16	7 Dec 2012 02:45	7 Dec 2012 04:21	PREC	2	7	–	–	–	–	–	–	–	–	3770
campaign median:				1	62	0.03	0.08[5]	261[5]	450	2.6	5322	2310	0.69	9553
				2			0.05[5]	364[5]						

[1]The wet activation threshold diameter represents the minimum of the surface size distribution at RH=100 % (ambient conditions) between the two modes representing the non-activated but hydrated particles and the activated fog droplets. This is expected to be an upper limit estimated of the true threshold size at ambient RH. Thus, the corresponding D_{act}^{upper} and SS$_{peak}^{lower}$ are considered to be upper and lower limit estimates, respectively (see Sects. 3.7 and 3.6 for details).

[2]The dry activation diameter was determined from the difference between the interstitial and total dry number size distributions. The activation threshold size is underestimated because the interstitial inlet also removed the largest non-activated but hydrated aerosol particles. Thus, D_{act}^{lower} and the corresponding SS$_{peak}^{upper}$ are considered to be lower and upper limit estimates, respectively.

[3]Scattering coefficient in the diameter range from 17 nm to D_{thres}^{wet}.

[4]Scattering coefficient in the diameter range from D_{thres}^{wet} to ∼ 10 µm, see Sect. 4.3 for further explanation.

[5]The bias introduced by the fact that the interstitial inlet removed some of the non-activated but hydrated aerosol particles is larger for the measurements performed with the 1 µm-cut-off as opposed to those with the 2 µm-cut-off. Therefore, separate median values are provided for the two different cut-offs. The results obtained with the 2 µm-cut-off are closer to the true value.
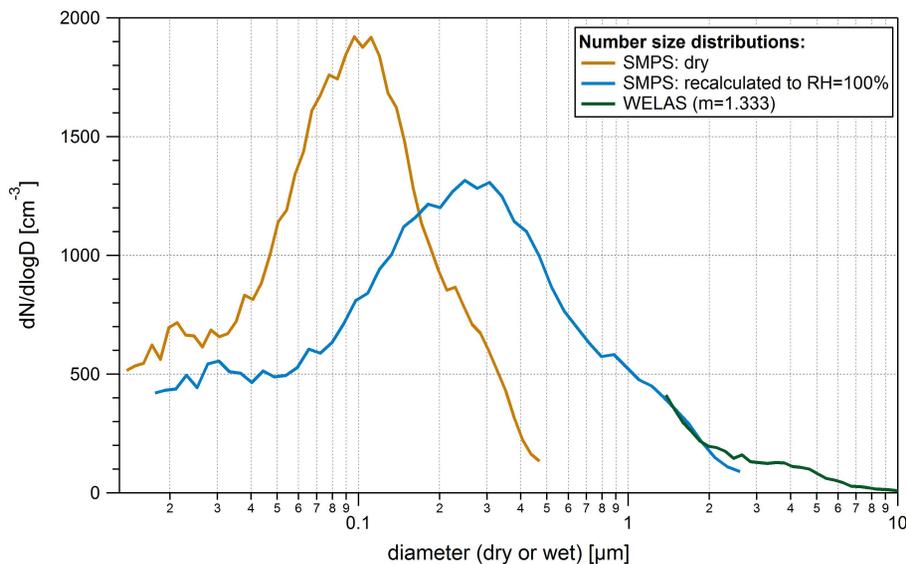
Fig. 1. For the fog event F9 on 12 November 2012: averaged dry total aerosol dry number size distribution (brown) measured by the SMPS and corresponding ambient wet number size distribution (blue) recalculated to RH = 100 % assuming a hygroscopicity parameter κ of 0.14. The ambient aerosol and fog droplet number size distribution (green) was measured with a WELAS (using the refractive index of pure water, $m = 1.333$, for the optical sizing).
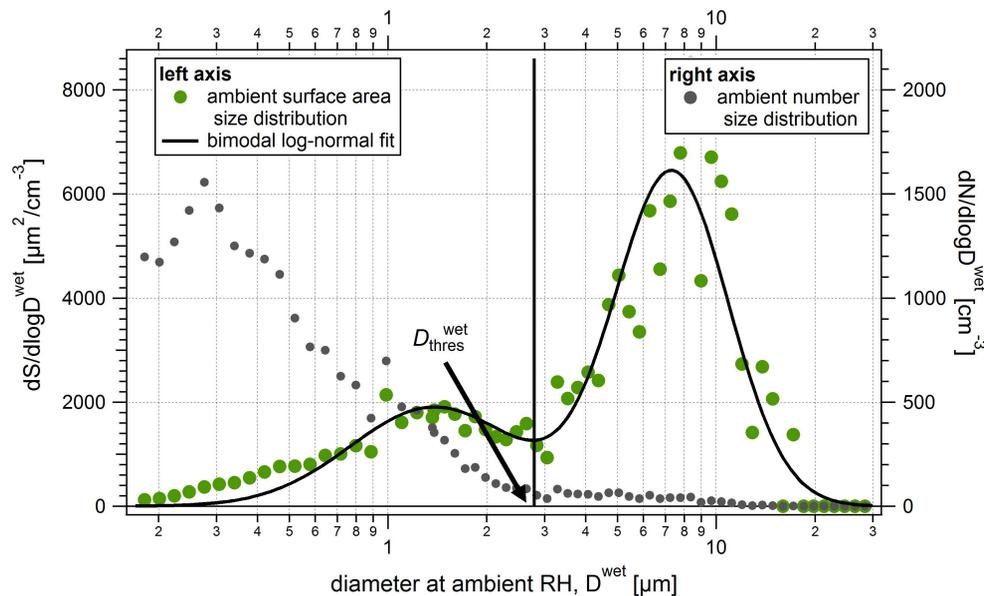
Fig. 2. For the fog event F9 on 12 November 2012 04:45: 12 min average number and surface area size distribution at ambient RH from the merged SMPS (recalculated to RH of 100 %) and WELAS measurement. Bimodal log-normal fit of the scattering coefficient was used to retrieve the D_{thres}^{wet}.
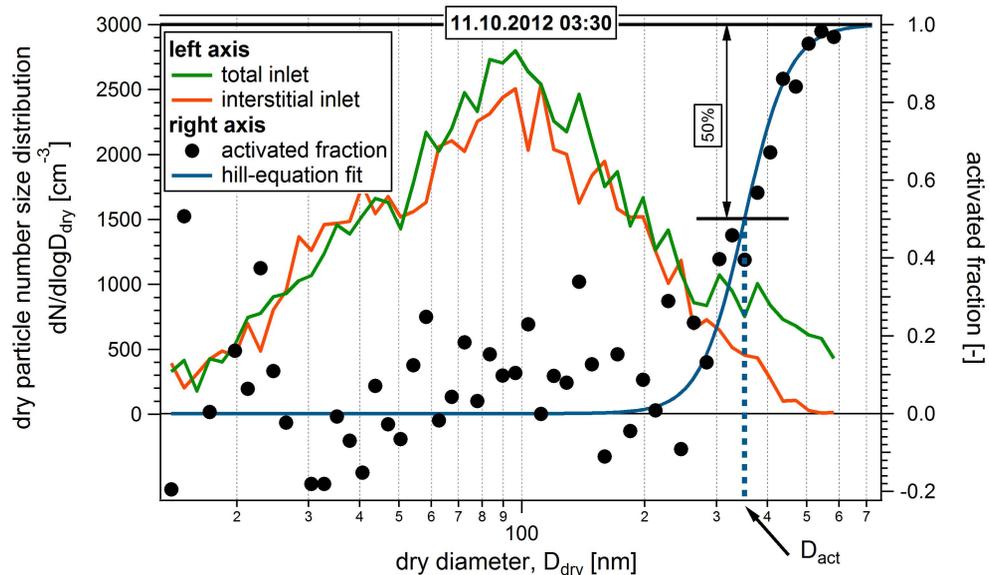
Fig. 3. 12 min average aerosol number size distributions measured behind the total (green) and interstitial (red) inlet for a developed fog event. The right axis shows the corresponding calculated activated fraction. The half-rise of the hill-equation fit (solid blue line) is defined as the dry activation diameter (D_{act}^{dry}; indicated with the blue dashed line), where 50 % of the particles were removed at the interstitial inlet because they grew above the cut-off of the impactor (2 µm), either due to activation to a fog droplet or due to a stable equilibrium diameter in the fog (RH ≈ 100 %) above the impactor cut-off.
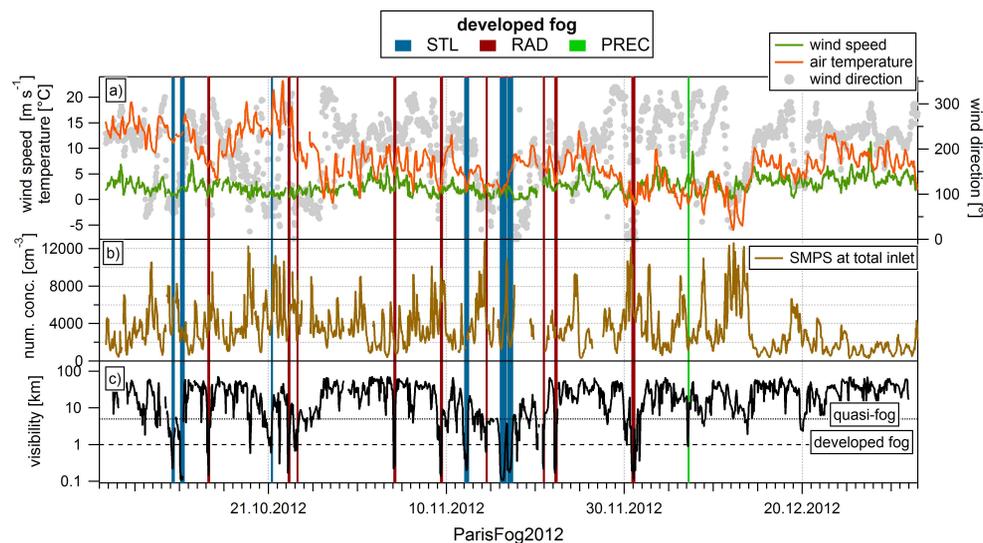
Fig. 4. All detected fog events (Stratus lowering fog; STL, radiation fog; RAD and precipitation fog; PREC) during ParisFog 2012/13 shown with: wind speed, wind direction and air temperature **(a)**, total particle number concentration **(b)** and visibility **(c)**.
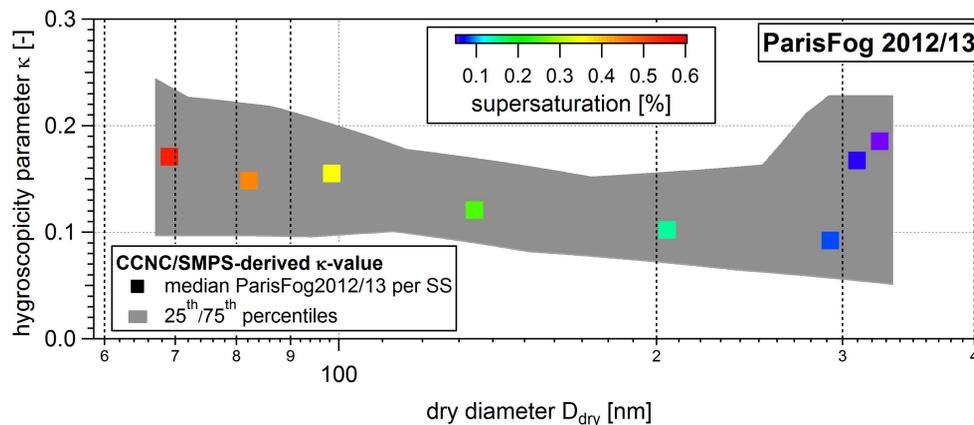
Fig. 5. Hygroscopicity parameter (κ) as a function of particle dry size during the ParisFog 2012/2013 campaign as derived from the polydisperse CCN and dry particle number size distribution measurements. The median values are given in color coded markers after supersaturation, and the 25th and 75th percentiles are indicated with gray shading.
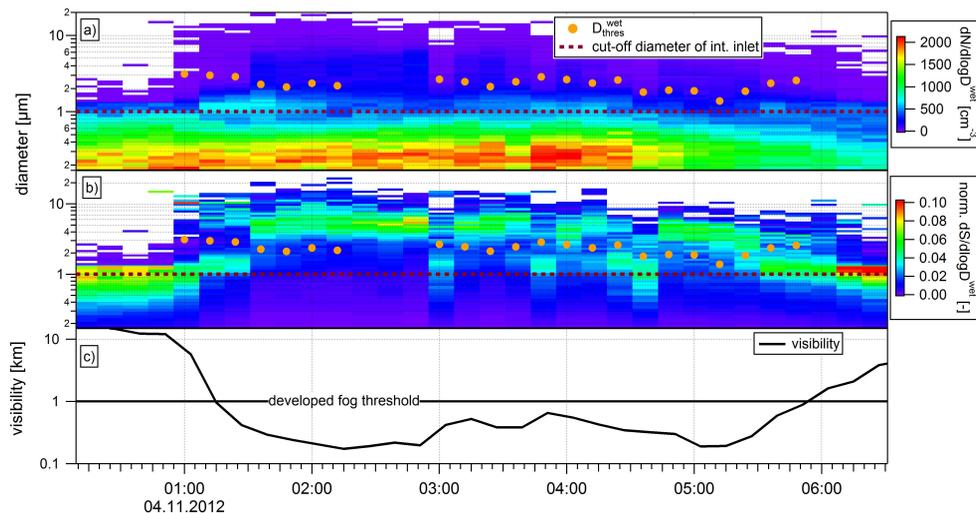
Fig. 6. Radiation fog event F7 observed at 4 November 2012. Ambient number size distribution ($\frac{dN}{d\log D^{wet}}$) obtained by combining the WELAS measurement (for $D^{wet} > 1.4\,\mu m$) merged with the SMPS measurement recalculated to RH=100 % (for $D^{wet} < 1.4\,\mu m$) **(a)**, the corresponding normalized ambient surface size distribution ($\frac{dS}{d\log D^{wet}}$) together with the wet activation threshold diameter (orange circles; D^{wet}_{thres}) and the cut-off diameter applied at the interstitial inlet (red dotted line) **(b)**, and the visibility measured by the Degreanne DF20+ forward scatter sensor **(c)**.
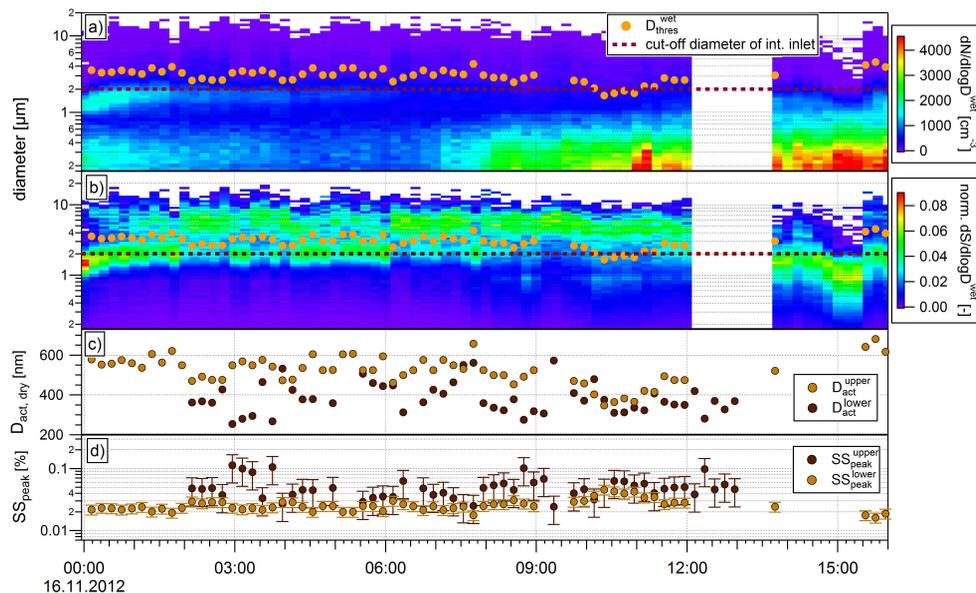
Fig. 7. Radiation fog event F11 observed at 16 November 2012. Ambient number size distribution ($\frac{dN}{d\log D^{wet}}$) obtained by combining the WELAS measurement (for $D^{wet} > 1\,\mu m$) merged with the SMPS measurement recalculated to RH=100 % (for $D^{wet} < 1\,\mu m$) **(a)**, the corresponding normalized ambient surface size distribution ($\frac{dS}{d\log D^{wet}}$) **(b)**, the dry activation diameters (D_{act}) **(c)** and the corresponding effective peak supersaturations (SS_{peak}) **(d)**. The error bars for SS_{peak}^{lower} and SS_{peak}^{upper} are explained in Sect. 3.7.
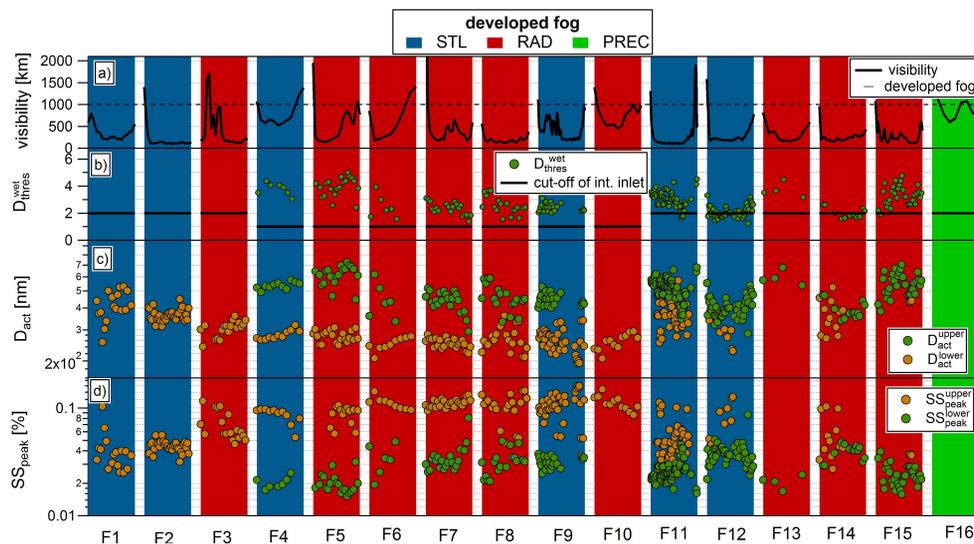
Fig. 8. Visibility **(a)**, wet activation threshold diameters **(b)**, dry activation diameters (D_{act}^{dry}) **(c)**, and effective peak supersaturation values (SS_{peak}) **(d)**.

Title Page

Abstract | Introduction

Conclusions | References

Tables | Figures

|◄ | ►|

◄ | ►

Back | Close

Full Screen / Esc

Printer-friendly Version

Interactive Discussion
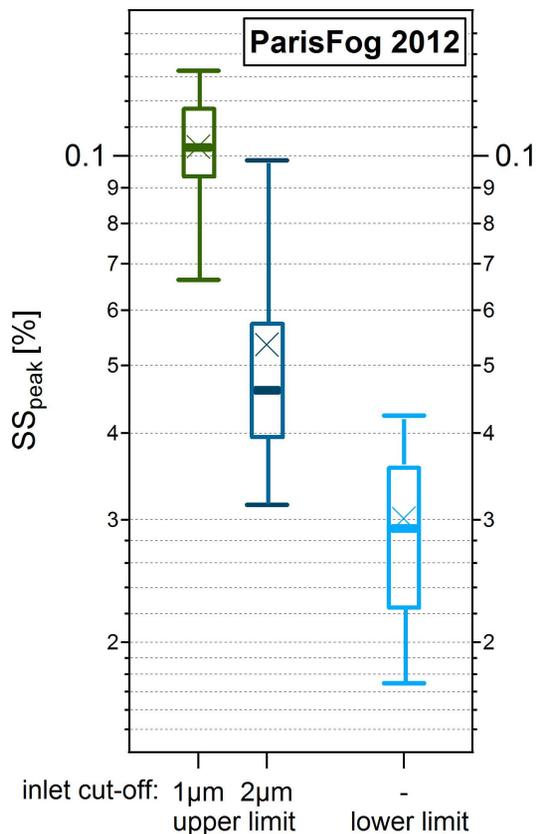
Fig. 9. 10th, 25th, 50th (median), 75th and 90th percentiles (boxplot) and mean value (cross) of the effective peak supersaturation (SS_{peak}) for the upper and lower estimate for ParisFog 2012/13. For the upper estimate the data was split according to the cut-off diameter at the interstitial inlet, 1 µm (PM_1) and 2 µm (PM_2).

Title Page

Abstract | Introduction

Conclusions | References

Tables | Figures

⏮ | ⏭

◀ | ▶

Back | Close

Full Screen / Esc

Printer-friendly Version

Interactive Discussion
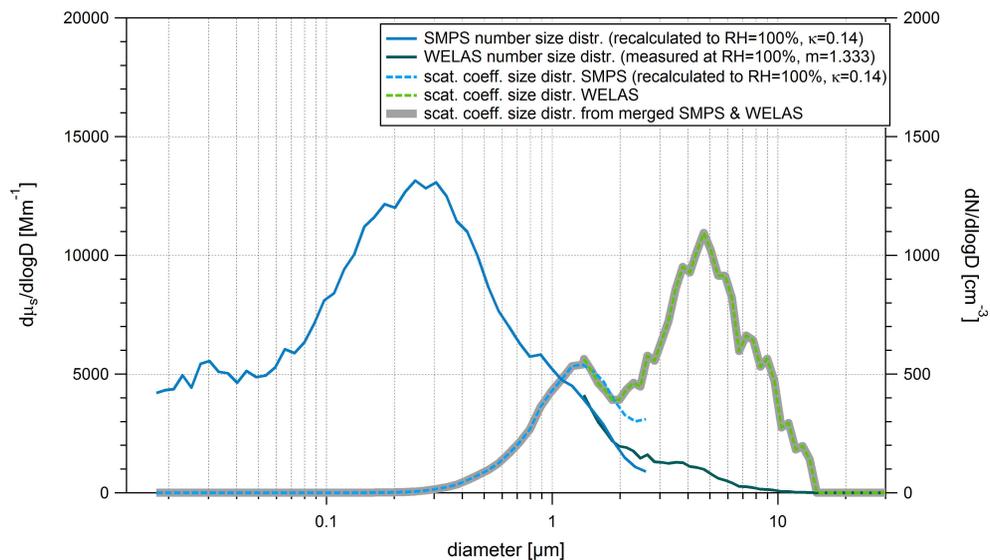
Fig. 10. For the fog event F9 on 12 November 2012: Averaged total aerosol number size distribution (solid blue) and ambient aerosol number size distribution measured by WELAS (solid green). Scattering coefficient size distribution of recalculated SMPS data for relative humidity (RH) of 100 % and hygroscopicity parameter κ of 0.14 (dashed blue), and for the WELAS data (dashed green). The solid grey line indicates the merged scattering coefficient size distribution from SMPS and WELAS data.